NUCL SCI TECH (2018) 29:143
https://doi.org/10.1007/s41365-018-0476-z

Generating femtosecond coherent X-ray pulses in a diffraction-limited storage ring with the echo-enabled harmonic generation scheme

Wei-Hang Liu[1,2] · **Guan-Qun Zhou**[1,2] · **Yi Jiao**[1]

Received: 19 January 2018 / Revised: 11 April 2018 / Accepted: 13 April 2018 / Published online: 30 August 2018

Abstract To study ultrafast processes at the sub-picosecond level, novel methods based on coherent harmonic generation technologies have been proposed to generate ultrashort radiation pulses in existing ring-based light sources. Using the High Energy Photon Source as an example, we numerically test the feasibility of implementing one coherent harmonic generation technology, i.e., the echo-enabled harmonic generation (EEHG) scheme, in a diffraction-limited storage ring (DLSR). Two different EEHG element layouts are considered, and the effect of the EEHG process on the electron beam quality is also analyzed. Studies suggest that soft X-ray pulses, with pulse lengths of a few femtoseconds and peak powers of up to 1 MW, can be generated by using the EEHG scheme, while causing little perturbation to the regular operation of a DLSR.

Keywords Echo-enabled harmonic generation · Diffraction-limited storage ring · High-energy photon source · Femtosecond X-ray pulses

This work was supported by National Natural Science Foundation of China (No. 11475202, 11405187), the Youth Innovation Association of Chinese Academy of Sciences, and Key Research Program of Frontier Sciences, CAS (No. QYZDJ-SSW-SLH001).

✉ Yi Jiao
jiaoyi@ihep.ac.cn

[1] Key Laboratory of Particle Acceleration Physics and Technology, Institute of High Energy Physics, Chinese Academy of Sciences, Beijing 10004, China

[2] University of Chinese Academy of Sciences, Beijing 100049, China

1 Introduction

The so-called diffraction-limited storage ring (DLSR) [1] is considered to be a candidate for the new generation of light sources, with natural emittance approaching the diffraction limit of X-rays, and is of interest to the science communities. Owing to the ultralow emittance in DLSRs, the brightness of synchrotron radiation can be improved by one or two orders of magnitude compared with the existing available third-generation light sources, providing potential promise for high-resolution imaging, microscopy and spectroscopy, and bringing new sciences in the corresponding scientific fields [2].

Note that without a special design, the radiation pulse duration available in a DLSR is usually of the same order as the bunch length of the electron beam, typically 10–100 ps. Consequently, the emitted photon beam is suitable only for material dynamics experiments on the picosecond timescale. To study ultrafast processes with shorter time scales, for example, atomic vibrational and electron–electron collisions in solids [3], sub-picosecond coherent radiation pulses are required.

To date, many novel methods have been proposed to achieve sub-picosecond radiation pulses in ring-based light sources. One method is to select a small fraction of the electrons from a long electron bunch and use them for spontaneous radiation to achieve a sub-picosecond photon beam [4–6]. Nevertheless, the output radiation is incoherent longitudinally. Another method based on the coherent harmonic generation technologies, e.g., the standard coherent harmonic generation (CHG) [7] scheme, echo-enabled harmonic generation (EEHG) [8–11], and phase-merging enhance harmonic generation (PEHG) [12, 13], can be used to enhance the longitudinal coherence. These schemes have been widely applied in seeded free electron lasers (FELs) and storage rings. In this method, the energy modulation in the electron bunch is introduced by means of an external laser interacting with the electron beam in an undulator (called a modulator). This converts the energy modulation into a density modulation by electron beam passing through a dispersion section (e.g., a 4-bend chicane), before sending the electron beam to the downstream undulator (called a radiator) to generate a high-power photon beam. Compared with the standard CHG scheme, which has one modulator, one dispersion section and one radiator, the PEHG and EEHG schemes are capable of generating higher harmonic radiation with a smaller energy modulation. The PEHG scheme needs an additional dispersive structure (e.g., a dogleg), and in this scheme the modulator is a transverse gradient undulator. The EEHG scheme additionally needs a modulator and dispersion section to generate energy bands in phase space.

In the PEHG scheme, the modulators are required to be located within a dispersive transfer line. However, in the DLSR designs the long straight sections are usually designed to be dispersion-free. Consequently, to implement PEHG in a DLSR, it is necessary to re-match the optics of straight sections where the PEHG elements are to be placed. However, this may destroy the lattice periodicity and increase the difficulty of nonlinear optimization. A delicate design and optimization of the lattice is necessary.

In the EEHG scheme by contrast, it is best to place the elements within a dispersion-free transfer line. This makes it possible to implement EEHG in a DLSR without a great change in the lattice. In the following sections, using the High Energy Photon Source (HEPS) as an example, we will discuss the concrete implementation of EEHG in a DLSR. In Sect. 2, two different EEHG element layouts are studied and the corresponding radiation performance is compared. Note that the radiation pulse is typically of the same order of the seed laser. Nevertheless, in Sect. 3, we will show that with some modifications, it is feasible to generate a radiation pulse with a much shorter duration compared to the seed laser. In Sect. 4, the effects of the EEHG process on the electron beam and daily operation of the light source are discussed. The conclusions are given in Sect. 5.

2 Two different element layouts of the EEHG scheme

Two different element layouts of the EEHG scheme, i.e., locating the EEHG elements in one or two straight sections, are considered; the schematic layouts are shown in Fig. 1, and element parameters are listed in Table 1.

Taking one HEPS design [14] as an example, we evaluate the radiation performance with the EEHG scheme. For this design, the natural emittance is 60 pm. In the following study, a coupling factor of 10% (ratio of the vertical to horizontal emittances) is assumed. The main parameters of this design are listed in Table 1. In addition, we use the Genesis program [15] to simulate the energy modulation and radiation process and use the Elegant program [16] to track particles through the beam line (e.g., the chicane and arc lattice), taking into account the coherent synchrotron radiation (CSR) and incoherent synchrotron radiation (ISR) effects.

2.1 Implementing EEHG in one straight section

As shown in Fig. 1a, all EEHG elements, including the two modulators, two dispersion sections and one radiator, are placed in one 6-m straight section. To maximize the radiator length, as well as the output radiation power, much attention is paid to minimize the lengths of the modulators and chicanes.

For both dispersion sections, we consider the use of 4-dipole chicanes, each of which has a positive R_{56}. Reference [17] described how to obtain the optimal values of EEHG parameters resulting in a maximum bunching factor for such an EEHG layout. Following Ref. [17], the bunching factor in a 1-D approximation can be written of the form,

$$b_{nm} = \left| e^{-(1/2)[nB_1+(m+n)B_2]^2} J_m[-(m+n)A_2B_2] \times J_n\{-A_1[nB_1+(m+n)B_2]\} \right|, \tag{1}$$

where n and m are integer numbers; $A_i = \Delta\gamma_i/\sigma_\gamma$ and $B_i = R_{56}^{(i)}k_s\sigma_\gamma/\gamma$ are the dimensionless parameters, with $i = 1, 2$; $\Delta\gamma$ is the energy modulation amplitude; σ_γ is the beam energy spread; $R_{56}^{(i)}$ is the longitudinal dispersion of the ith chicane; $k_s = 2\pi/\lambda_s$, and λ_s is the wavelength of the seed laser (assuming two seed lasers have the same wavelength); and γ is the Lorentz factor of the electron beam.

The bunching factor reaches its maximum when $n = \pm1$, and $n \times m \times B_1 \times B_2 < 0$. In this case, $B_1 \times B_2 > 0$, so $n \times m < 0$. One can choose $n = 1$ and $m < 0$, or $n = -1$ and $m > 0$. While the harmonic conversion number $N = n + m$ should be a positive integer. Thus, for this case the only choice is $n = -1$ and $m > 0$.

Under these conditions, Eq. (1) can be simplified to:

$$\begin{aligned} b_N &= \left|J_{N+1}[-NA_2B_2] \times J_1[\xi A_1]\exp(-\xi^2/2)\right| \\ &= |J_{N+1}[-NA_2B_2]|F(\xi, A_1), \end{aligned} \tag{2}$$

where $\xi = B_1 - NB_2$, $N = m - 1$, and $F(\xi, A_1) = J_1(\xi A_1)\exp(-\xi^2/2)$.

When $N > 3$, the maximal value of function $J_{N+1}(NA_2B_2)$ is $\sim 0.67/(N+1)^{1/3}$, which is achieved when

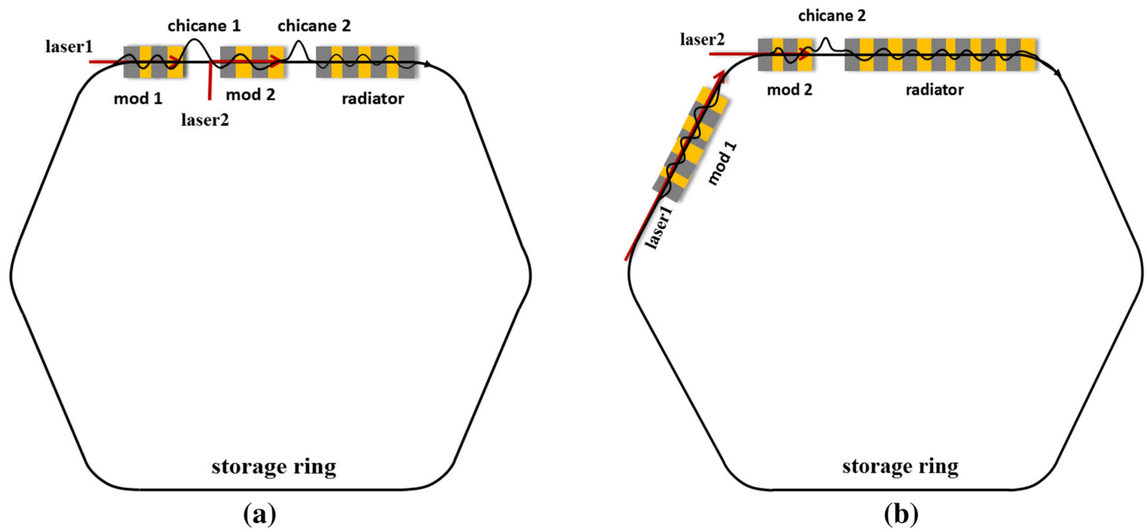

Fig. 1 (Color online) Schematic layout of the two cases; **a** the modulator and radiator are placed on the same straight section and **b** the modulator and radiator are placed on the adjacent straight section, with the arc region taken as the first dispersion section (*mod* modulator)

$$NA_2B_2 = (N+1) + 0.81(N+1)^{1/3}. \tag{3}$$

When A_2 and B_2 satisfy Eq. (3), Eq. (2) can be written as:

$$b_N = \frac{0.67}{(N+1)^{\frac{1}{3}}} F(\xi, A_1). \tag{4}$$

For a specific A_1, one can obtain the maximum value of $F(\xi, A_1)$ and correspondingly the available maximum bunching factor. In our study, we choose $N = 30$. The optimized bunching factor b_{30} with different A_1 is shown in Fig. 2. It is feasible to achieve larger b_{30} with larger A_1. On the other hand, the laser-induced energy spread is proportional to the square root of $(A_1)^2/2 + (A_2)^2/2$. To avoid a too large energy spread, A_1 cannot be too large. In our study, we set A_1 to 3, with the corresponding optimal value of ξ as $\xi_{opt} = 0.45$.

From Eq. (3) and the relation $\xi = B_1 - NB_2$, the corresponding optimal values of B_1 and B_2 can be calculated for a specific A_2. From Eq. (3), the optimal value of B_2 (the R_{56} of the second chicane) is inversely proportional to A_2. Considering that a small B_2 implies a small chicane length, we reduce the required R_{56} of the chicane by choosing a large A_2 to obtain a chicane with a small enough length.

For this case, previous studies showed that B_2 decreases drastically when A_2 is smaller than 1, but decreases slowly when A_2 is larger than 1. Therefore, we choose $A_2 = 1$. From Eq. (3) and $\xi = B_1 - NB_2 = \xi_{opt}$ we find that $B_1 = 26.4$ and $B_2 = 0.86$. With these parameters and the compact structure of the chicane, i.e., without the drift space between adjacent bend magnets, we control the total length of the space taken by the EEHG elements to be 5.3 m but with a 1-m radiator. The detailed parameters are listed in Table 1.

In general, the ISR effect in the dispersion section 1 and CSR effect in the dispersion section 2 may affect the performance of the EEHG scheme. In order to verify the rationality of the parameters, we use Eq. (12) in Ref. [17] to calculate the energy spread caused by the ISR effect of chicane 1, which is $\sim$ 77 keV. The smallest spacing between the energy bands ΔE_{gap} is $\sim$ 288 keV. It is apparent that the energy band is larger than the ISR-induced energy spread. Using Eq. (38) in Ref. [18], we calculate the CSR-induced final gain, G_f, of the density modulation in chicane 2. It turns out that $G_f \sim 0$ when the modulation wavelength is smaller than 1 μm. In this paper, the modulation wavelength is 240 nm, so the CSR effect is negligible.

With these parameters, the longitudinal phase space evolution of the electron bunch in one seed wavelength range simulated with the Elegant program is shown in Fig. 3. A microbunching structure is clearly produced at the end of the second chicane. The simulation results of the radiation performance with Genesis (time-dependent mode) are shown in Fig. 4. The radiation power is $\sim$ 200 kW, with a full width at half maximum (FWHM) duration of $\sim$ 26 fs. The central wavelength is 8 nm, with a FWHM bandwidth of 0.05%.

For comparison, we consider the radiation from a 5.5-m undulator that is filtered with an ideal grating monochromator (without energy loss) at an 8 nm wavelength with spectral bandwidth of $\sim$ 0.1%. The output peak power is only $\sim$ 200 W, and the duration of the radiation pulse is $\sim$ 16 ps.

Table 1 EEHG parameters at HEPS

Parameters	Value
Beam energy (GeV)	6
RMS of the relative energy spread (%)	0.08
RMS bunch length (mm)	2.07
RMS of the horizontal emittance (pm rad)	55
RMS of the vertical emittance (pm rad)	5.5
Peak current (A)	70
Length of the straight section (m)	6
Period of Mod 1/Mod 2 (m)	0.15/0.15
Radiator period (cm)	5
Radiation wavelength (nm)	8
Implementing EEHG in one straight section	
Peak power of the seed laser 1 (GW)	98
Peak power of the seed laser 2 (GW)	24
Rayleigh length of the seed laser 1/2 (m)	1
Seed wavelength (nm)	240
FWHM of the seed pulse duration (fs)	50
First chicane R_{56} (mm)	1.25
First chicane length (m)	2.12
Second chicane R_{56} (μm)	41.23
Second chicane length (m)	0.68
Period number of Mod 1/Mod 2	6/4
Period number of radiator	20
Implementing EEHG in two adjacent straight sections	
Peak power of the seed laser 1 (GW)	35
Peak power of the seed laser 2 (GW)	15
Rayleigh length of the seed laser 1/2 (m)	1
Seed wavelength (nm)	240
FWHM of the Seed pulse duration (fs)	50
Arc region R_{56} (mm)	− 1
Chicane R_{56} (μm)	32.41
Chicane length (m)	0.85
Period number of Mod 1/Mod 2	9/6
Period number of radiator	80

RMS root mean square, *FWHM* full width at half maximum

2.2 Implementing EEHG in two adjacent straight sections

Similar to the element layout shown in Ref. [10], in this case, we consider placing the EEHG elements in two adjacent 6-m straight sections. In particular, we use the arc region between these two straight sections as the first dispersion section.

The purpose of the dispersion section in EEHG is to convert the energy modulation to density modulation with an appropriate value of R_{56}. It is best for this section to have small x–z coupling terms, such as R_{51} and R_{52}, to

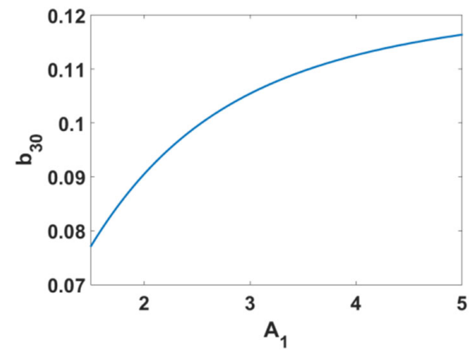

Fig. 2 The optimized bunching factor at the 30th harmonic of the seed laser for different values of A_1

minimize perturbations of this process to the transverse distribution of electrons. The DLSR lattice intrinsically satisfies this requirement, based on the fact that the DLSR lattice has been designed to have small dispersion functions, R_{16} and R_{26}, to achieve ultralow natural emittance, and correspondingly small R_{51} and R_{52} according to the symplectic conditions $R_{51} = R_{26}$ and $R_{52} = -R_{16}$. Tracking results show that the energy bands emerge when $R_{51} < 7 \times 10^{-4}$ and $R_{52} < 1$ mm and in the lattice of the HEPS, $R_{51} = R_{26} = 4 \times 10^{-8}$ and $R_{52} = -R_{16} = 10^{-3}$ mm, satisfying the conditions to generate the energy bands.

To simplify the element layout and different from Ref. [10], we use a 4-bend chicane as the second dispersion section, rather than a section with R_{56} of the same sign as the arc region. In the latter case, the second dispersion section is more complex and also requires a longer straight section.

In this case, the conditions for the parameter optimizing of the EEHG scheme are different from those in Sect. 2.1, i.e., $B_1 \times B_2 < 0$, $n = 1$, $m > 0$, and B_1 is a fixed value that is related to the arc design of the DLSR (for HEPS, $B_1 = -21$).

Starting from Eq. (1) and using a similar procedure to that in Ref. [17], we find that the bunching factor is still proportional to the function $F(\xi, A_1)$, while in this case $\xi = B_1 + NB_2$ with $N = m + 1$. Again, we choose $N = 30$. The optimal conditions for A_2 and B_2 are then changed to

$$\begin{cases} \xi_{\text{opt}} = B_{1,\text{opt}} + NB_{2,\text{opt}} \\ A_{2,\text{opt}} = \dfrac{(N-1) + 0.81(N-1)^{\frac{1}{3}}}{NB_{2,\text{opt}}} \ (N > 5) \end{cases}. \tag{5}$$

In this case, we have more space to place the radiator compared to that in Sect. 2.1. Somewhat arbitrarily, we set A_1 to 2.2, to obtain enough energy modulation to maximize the bunching factor, with a small induced energy spread. From Eq. (5), we obtain $A_{2,\text{opt}} = 1.5$ and $B_{2,\text{opt}} = 0.72$. In this case, one can also choose $A_1 = 3$ as in Sect. 2.1 which,

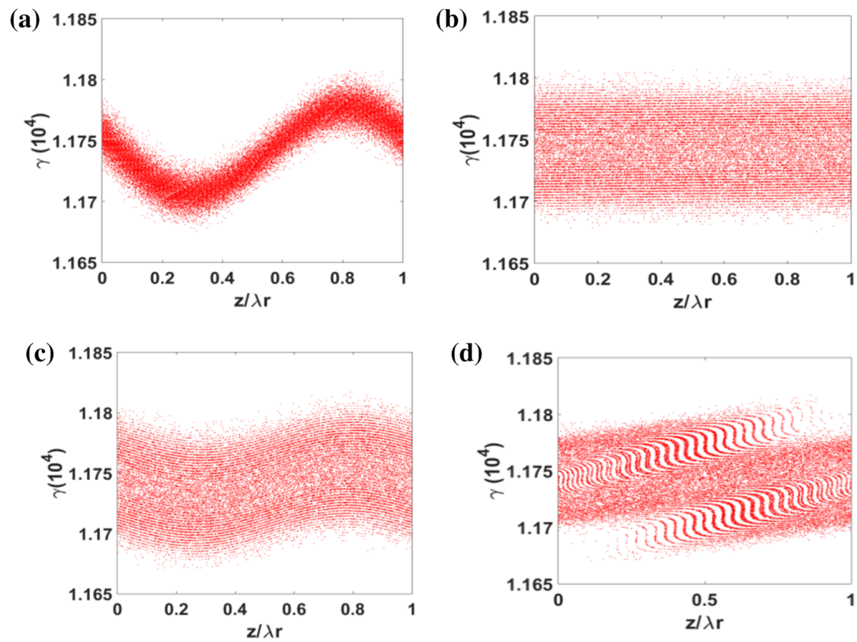

Fig. 3 (Color online) Longitudinal phase space evolution at optimal parameters in one wavelength range; **a** after modulator 1, **b** chicane 1, **c** modulator 2, and **d** chicane 2

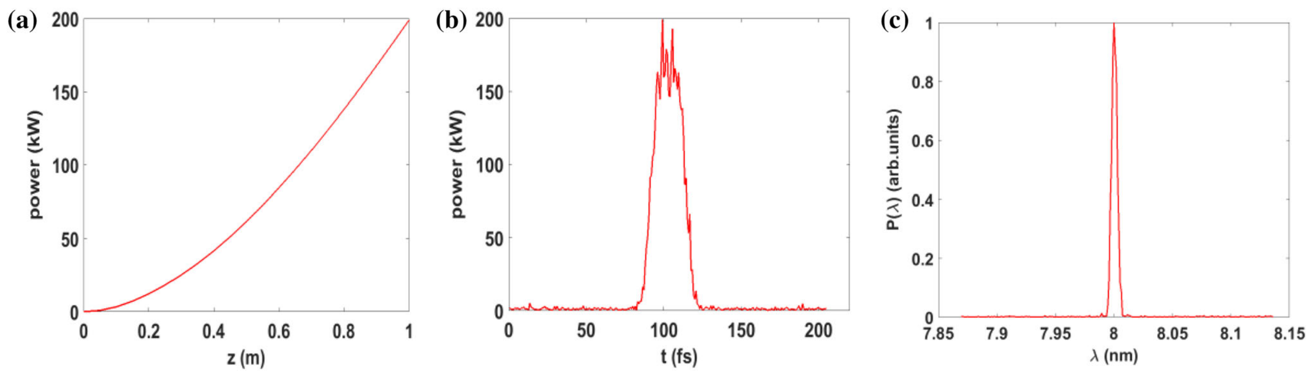

Fig. 4 (Color online) **a** Evolution of the peak power along the undulator. Distribution of the radiation output in the **b** time domain and **c** spectrum domain, when locating all EEHG elements in one 6-m straight section obtained with the Elegant and Genesis simulation

however, does not cause a huge difference in the output power.

However, studies show that these values of parameters result in a maximum bunching factor at the entrance of the radiator, but not the maximum output power from the radiator. This is because with the EEHG scheme in a ring-based light source, the radiation works in the coherent radiation regime. In this regime, the radiation power is determined by the integral of b_N along the radiator, rather than the b_N at a specific location [19, 20]. In this case, the radiator length, L = 4 m, is much longer than that used in Sect. 2.1. In radiator the bunching factor has an evident change when the electron beam passes through the radiator.

To obtain a maximum output power, one needs to optimize the parameters so that the bunching factor reaches a maximum near the center of the radiator. This means that for $R_{56}^{(2)}$, the R_{56} of the chicane and half of the undulator needs to be taken into account. In this way, we calculate the optimal R_{56} of the second chicane by

$$R_{56,\mathrm{opt}}^{(2)} = R_{56}^{(2)*} - \frac{2\pi}{\lambda_\mathrm{u}}\frac{L}{N}\frac{\Delta\gamma}{\sigma_\gamma k_\mathrm{s}}, \tag{6}$$

where $R_{56}^{(2)*} = B_{2,\mathrm{opt}}\ \gamma/(k_\mathrm{s}\sigma_\gamma) = 34.4$ µm, $\lambda_\mathrm{u} = 5$ cm is the period of the radiator, and $\Delta\gamma = 234.8$ is the laser-induced energy spread. By Eq. (6), the optimal $R_{56}^{(2)}$ is $\sim$ 32.8 µm.

To verify, we scan $R_{56}^{(2)}$ and the dimensionless undulator parameter K and use Genesis (steady-state mode) to calculate the radiation power. The results are shown in Fig. 5. The optimal $R_{56}^{(2)}$ is 32.5 µm, which agrees well with the analytical prediction. The optimal deviation of K is $\Delta K/K_0 = (K - K_0)/K_0 = -0.5\%$ ($K_0 = 9.3$).

Before the simulation, we estimate the ISR-induced energy spread in dispersion section 1 as $\sim$ 11.2 keV, which is much smaller than the gap of the energy bands

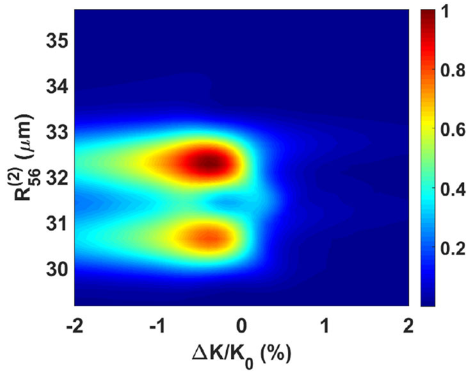

Fig. 5 (Color online) Calculated radiation power (arb. units) as a function of $R_{56}^{(2)}$ and $\Delta K/K_0$. When $R_{56}^{(2)}$ is $\sim$ 32.5 μm and $\Delta K/K_0 = -0.5\%$, the maximum power can be achieved. The change of color from blue to red corresponds to an increase in radiation power from low to high

$\Delta E_{gap} \sim$ 355 keV. The CSR-induced final gain G_f of the density modulation in the second chicane is calculated by the same way, as shown in Sect. 2.1. We find that $G_f \sim 0$ at the modulation wavelength of 240 nm. Therefore, the selected parameters are appropriate.

The simulation results of the radiation performance are shown in Fig. 6. Compared to the case in Sect. 2.1, due to the adoption of 4 times longer radiator, it is feasible to increase the peak power by $\sim$ 6 times, to $\sim$ 1.2 MW.

Note that in this case, one HEPS arc was used as the first dispersion section, containing many quadrupoles. The path length differences for the electrons with different betatron amplitudes may smear out the longitudinal density modulation (see, for example, Refs. [21, 22]). To estimate the influence of the microbunching structure by this effect, we track a bunch with zero initial bunch length and zero initial energy spread through the first modulator (without laser-beam interaction), arc section, the second modulator (without laser-beam interaction), and the second chicane (The bending angles are set to zero). We find the final RMS bunch length is $\sim$ 0.37 nm. In this study, the radiation wavelength is 8 nm. The smearing effect is negligible. However, for the shorter wavelength, e.g., 0.5–1 nm, this effect may greatly reduce the bunching factor.

3 Generating a radiation pulse much shorter than the seed laser

As shown in Sect. 2, the radiation pulse length ($\sim$ 25 fs FWHM) is similar to that of the seed laser (50 fs FWHM). To further reduce the length of the radiation pulse, e.g., to a few femtoseconds, a seed laser with a shorter pulse length can be used to modulate the electron beam. However, the wavelength of the state-of-the-art high-power, femtosecond laser pulse is limited to $\sim$ 600 nm [23], causing difficulties in generating soft X-ray pulses with EEHG.

We introduce here a way of achieving radiation pulses much shorter than the seed laser with some small changes in the EEHG scheme. As shown in Fig. 7a, in the EEHG scheme the timing of the two seed lasers is usually adjusted such that the maximum fields of both seed lasers interact with the electrons at the same temporal location. As shown in Fig. 7b, if the two seed lasers are not perfectly overlapped relative to the electron bunch, but with their peaks separated by a small time duration, only some of the electrons will experience effective modulations from both lasers (see the shadowed area of Fig. 7b). As a result, the microbunched electrons display a shorter length compared with the normal case (see Fig. 7a).

To find the appropriate displacement of the two seed lasers, we assume that the power profile of the seed laser is Gaussian with a pulse duration of σ_t and the displacement is Δt in units of σ_t. By Eq. (2) and the parameters from Sect. 2.2, we find the bunching factor for different Δt, shown in Fig. 8a. By the approximation output power $\sim$ constant $\times$ b_N^2, the output radiation pulse for different Δt is shown in Fig. 8b, in which we can see that when Δt increases, the FWHM pulse length is decreased. To obtain a radiation pulse with a pulse length that is approximately one order lower than the duration of the

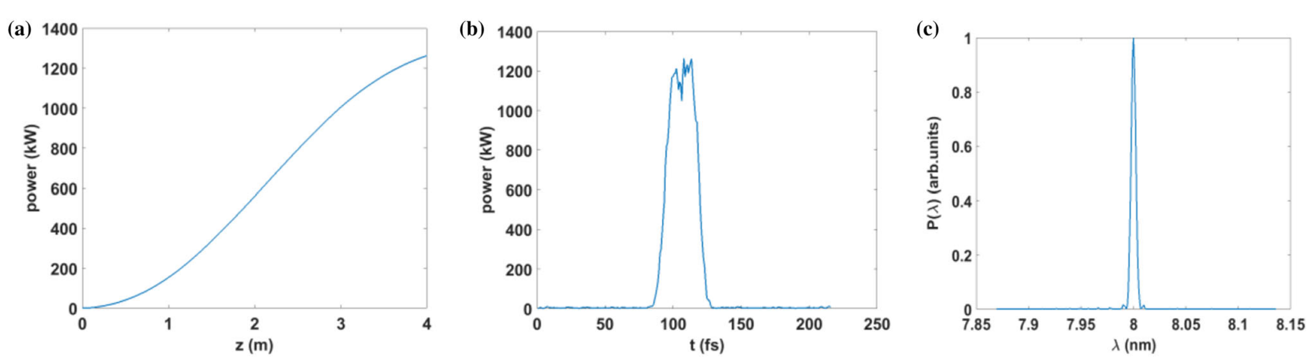

Fig. 6 aEvolution of peak power along the undulator. Distribution of the radiation output in the **b** time domain and **c** spectrum domain, when locating the EEHG elements in two adjacent straight sections obtained with the Elegant and Genesis simulation

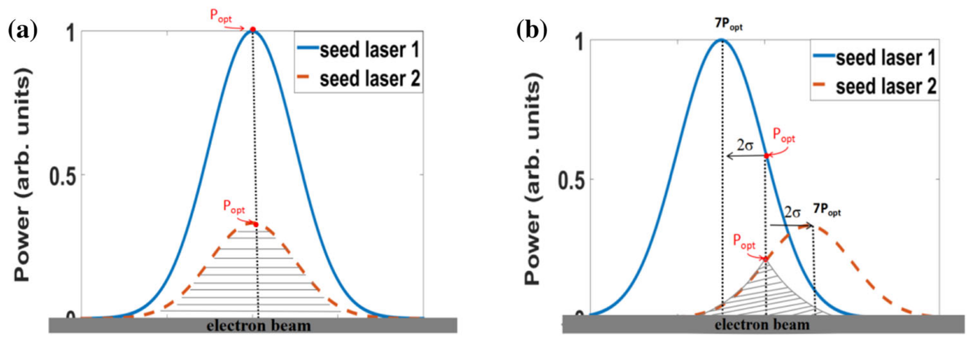

Fig. 7 (Color online) **a** EEHG scheme in the normal case in which the two seed lasers are perfectly overlapped relative to the electron beam and the peak power of the laser is used for beam energy modulation, **b** EEHG scheme to generate a much shorter radiation pulse than that of the seed laser, in which the two seed lasers are adjusted so that the two peak powers are separated by 2 times that of the laser pulse duration. The shadow area represents the effective modulation area of the EEHG scheme

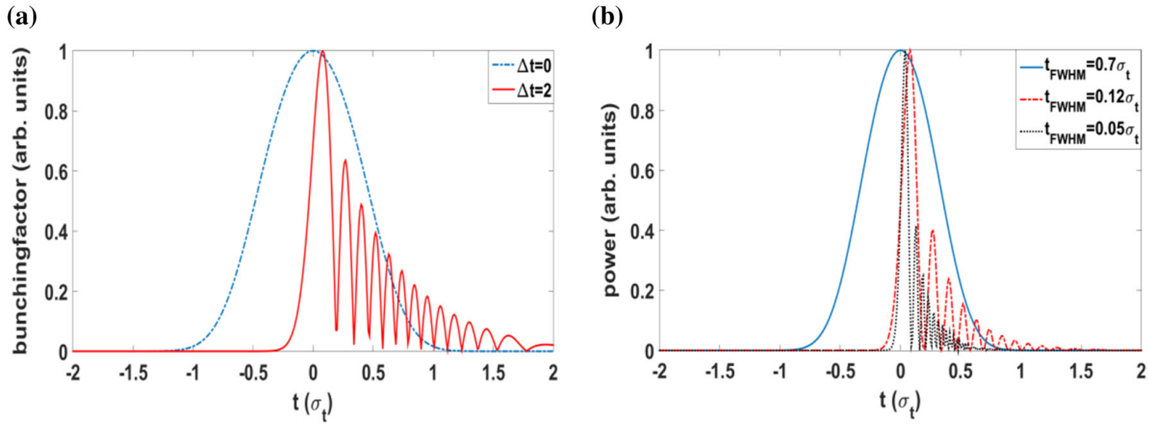

Fig. 8 (Color online) **a** Bunching factor along the electron bunch for various values of Δt. **b** Output radiation pulses for $\Delta t = 0$ with FWHM pulse length of $0.7\sigma_t$ (blue solid curve), $\Delta t = 2$ with FWHM pulse length of $0.12\sigma_t$ (red dash-dot curve) and $\Delta t = 4$ with FWHM pulse length of $0.05\sigma_t$ (black dot curve)

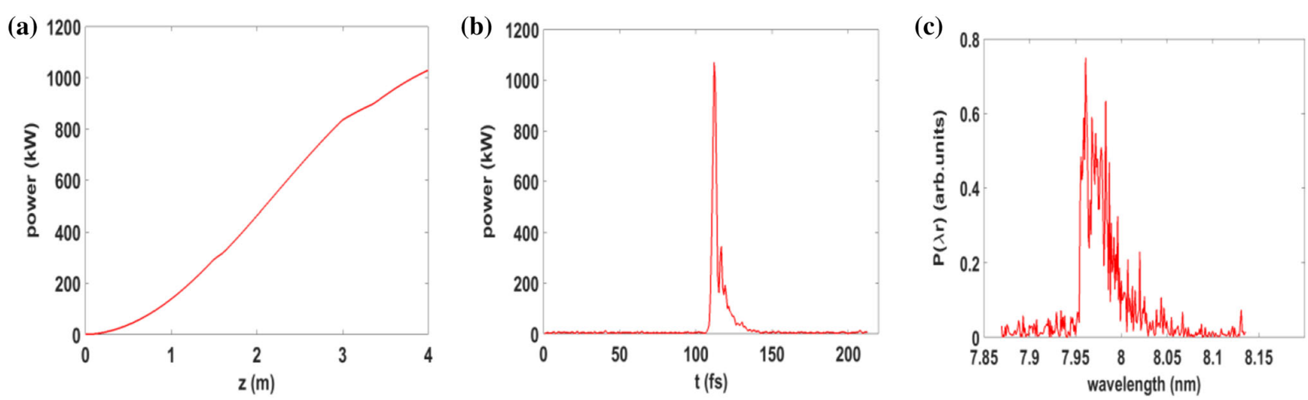

Fig. 9 (Color online) **a** Evolution of peak power along the undulator. Distribution of the radiation output in the **b** time domain and **c** spectrum domain, for a few femtoseconds pulse EEHG scheme, obtained with the Elegant and Genesis simulation

seed laser, from Fig. 8b, we know that Δt needs to be greater than 2. But a large Δt requires a large seed laser power, potentially inducing a large energy spread. So, in this paper, we choose $\Delta t = 2$.

The price is that a higher seed power is needed. As shown in Fig. 7b, the optimal seed power (P_{opt}) has the same value with the peak power of the normal case (Fig. 7a). For example, in this case, P_{opt} = 35 and 15 GW are required for the first and second seed lasers, with a peak

Table 2 Radiation simulation results

Parameters	Value
First case (Sect. 2.1)	
Radiation wavelength (nm)	8
Radiation peak power (MW)	0.2
FWHM pulse duration (fs)	26
FWHM spectral bandwidth (%)	0.05
Second case (Sect. 2.2)	
Radiation wavelength (nm)	8
Radiation peak power (MW)	1.2
FWHM pulse duration (fs)	25
FWHM spectral bandwidth (%)	0.05
Results from Sect. 3	
Radiation wavelength (nm)	8
Radiation peak power (MW)	1.0
FWHM pulse duration (fs)	2.4
FWHM spectral bandwidth (%)	0.4

power of $\sim$ 7 times larger than that of the normal case (Fig. 7a).

We use the same element layout of the EEHG scheme and seed laser pulse as for the case in Sect. 2.2, with the higher seed laser powers, i.e., 245 and 105 GW for the first and second seed lasers, respectively.

The simulation results of the radiation performance are shown in Fig. 9. Compared with the results obtained in Sect. 2.2, the output radiation peak power is at the same level, $\sim$ 1 MW (Fig. 9a); the FWHM pulse length is approximately one order of magnitude shorter, $\sim$ 2.4 fs (Fig. 9b); and the spectral bandwidth is one order of magnitude larger, $\sim$ 0.4% (Fig. 9c). Compared with the spectrum shown in Fig. 6c, the spectrum in Fig. 9c has many spikes. Due to the longitudinal asymmetric modulation of the beam energy (see Fig. 7b), the bunching factor has many different peak values along the bunch, as shown in Fig. 8a. When passing the radiator, these electrons near the different peak values radiate at different longitudinal modes, generating many spikes in the spectrum. The main results of the three different cases are listed in Table 2.

4 Effect of the EEHG process

In general, the EEHG process will disturb the electron beam parameters, especially the emittance and energy spread. If these parameters exceed the acceptance of the storage ring, the beam will be unstable and get lost. In this section, we calculated the emittance and energy spread distortion after the EEHG process.

The results are shown in Fig. 10. The maximal value of the energy spread, $\delta_{\max}$, is 0.22% for the case in Sect. 2.1 and 0.2% for the case in Sect. 2.2 (Fig. 10a), which is much smaller compared to the momentum acceptance (MA) of the HEPS design that is $\sim$ 2.4% [24].

Figure 10b, c shows the fluctuations of the sliced and average (averaged over the slice emittance) emittances in the *x* and *y* planes, respectively. The relative increase of the emittance, $\Delta\varepsilon/\varepsilon$, is lower than 2% for both cases.

The above results are based on a one-pass EEHG scheme. To implement EEHG in a storage ring, a multi-pass EEHG operation mode must be considered.

We consider the case where EEHG is implemented once after one damping time (20 ms), corresponding to a repetition rate of $\sim$ 50 Hz. After one-pass of EEHG, the relative increase of the emittance is $\Delta\varepsilon/\varepsilon \sim 2\%$ and maximal value of the energy spread is $\delta_{\max} \sim 0.2\%$. After one damping time, $\Delta\varepsilon/\varepsilon$ and $\delta_{\max}$ are reduced to $\sim$ 0.74% and $\sim$ 0.074%, respectively, which may be tolerable in the daily operation of the HEPS.

In a storage ring, due to the quantum excitation and radiation damping, beam distortions can be completely

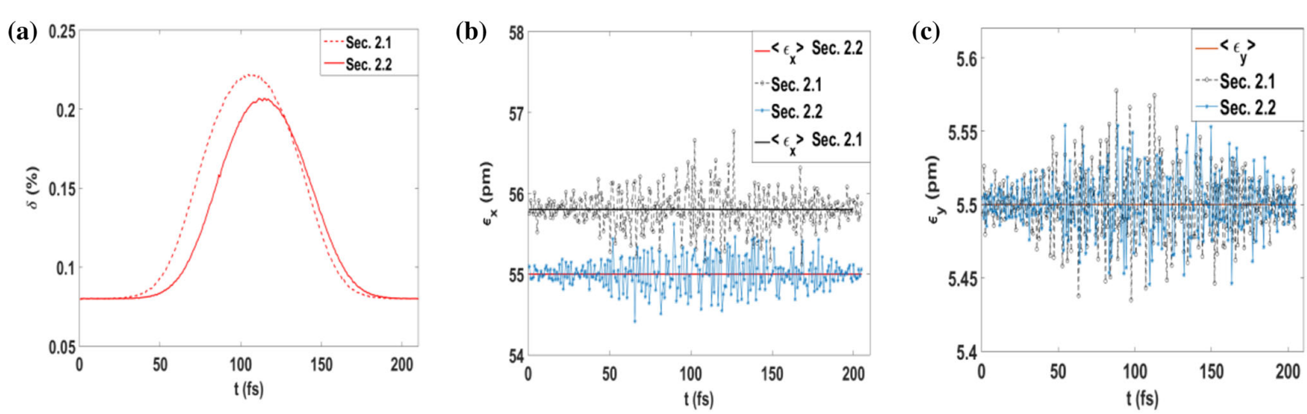

Fig. 10 (Color online) **a** Distribution of energy spread along the length of the bunch. Emittance in the **b** *x* and **c** *y* planes for the cases in Sects. 2.1 and 2.2

damped after 3 damping times. Therefore, the EEHG can be operated with a repetition rate of at least 16 Hz.

5 Conclusion

In this paper, the feasibility of implementing EEHG in a DLSR, based on a HEPS design, is studied. The results show that with the EEHG scheme it is feasible to obtain a photon beam with a peak power of up to 1 MW, approximately three orders of magnitude higher than the spontaneous undulator radiation, with pulse duration of about a few femtoseconds and the spectral bandwidth being close to the Fourier transform limit. The output photon beam can be used in an ultrafast process study.

We also analyzed the electron beam parameters distortions after the EEHG process. The main conclusion of this study is that the effect of the one-pass EEHG process on the beam parameters is very weak.

Finally, it is worth noting that because the beam energy of the HEPS is 6 GeV, the seed laser we used in this study has a high peak power. If a DLSR of moderate energy is used, for example a 3-GeV DLSR, the peak power of the seed laser will be approximately one-quarter lower.

Acknowledgements The authors would thank Dr. Chao Feng, Tong Zhang, Xiao-Yu Li, Xiao-Fan Wang, Zheng Qi, Hai-Xiao Deng, and Yi Wu for their helpful discussions.

References

1. R. Hettel, DLSR design and plans: an international overview. J. Synchrotron Radiat. **21**, 843–855 (2014). https://doi.org/10.1107/S1600577514011515
2. M. Eriksson, J.F. van der Veen, C. Quitmann, Diffraction-limited storage rings—a window to the science of tomorrow. J. Synchrotron Radiat. **21**, 837–842 (2014). https://doi.org/10.1107/S1600577514019286
3. J.D. Brock, Watching atoms move. Science **315**, 609–610 (2017). https://doi.org/10.1126/science.1136895
4. A.A. Zholents, M.S. Zolotorev, Femtosecond X-ray pulses of synchrotron radiation. Phys. Rev. Lett. **76**, 912 (1996). https://doi.org/10.1103/PhysRevLett.76.912
5. R.W. Schoenlein, S. Chattopadhyay, H.H.W. Chong et al., Generation of femtosecond pulses of synchrotron radiation. Science **287**, 2237–2240 (2000). https://doi.org/10.1126/science.287.5461.2237
6. S. Khan, K. Holldack, T. Kachel et al., Femtosecond undulator radiation from sliced electron bunches. Phys. Rev. Lett. **97**, 074801 (2006). https://doi.org/10.1103/PhysRevLett.97.074801
7. B. Girard, Y. Lapierre, J.M. Ortega et al., Optical frequency multiplication by an optical klystron. Phys. Rev. Lett. **53**, 2405 (1984). https://doi.org/10.1103/PhysRevLett.53.2405
8. G. Stupakov, Using the beam–-echo effect for generation of short-wavelength radiation. Phys. Rev. Lett. **102**, 074801 (2009). https://doi.org/10.1103/PhysRevLett.102.074801
9. R. Molo, M. Höner, H. Huck et al., EEHG and Femtoslicing at DELTA, in *Proceedings of FEL2013, New York*
10. C. Evain, A. Loulergue, A. Nadji et al., Soft X-ray femtosecond coherent undulator radiation in a storage ring. New J. Phys. **14**, 023003 (2012). https://doi.org/10.1088/1367-2630/14/2/023003
11. W. Gao, H. Li, L. Wang, Preliminary study of EEHG-based superradiant undulator radiation at the HLS-II storage ring. Chin. Phys. C **41**, 078101 (2017). https://doi.org/10.1088/1674-1137/41/7/078101
12. H. Deng, C. Feng, Using off-resonance laser modulation for beam-energy-spread cooling in generation of short-wavelength radiation. Phys. Rev. Lett. **111**, 084801 (2013). https://doi.org/10.1103/PhysRevLett.111.084801
13. F. Chao, B. Jiang, Z. Qi et al., Storage ring based PEHG FEL for EUV lithography storage ring based PEHG FEL for EUV lithography, in *Compact EUV X-ray Light Sources,* (2016), p. EM3A.1. https://doi.org/10.1364/euvxray.2016.em3a.1
14. G. Xu, J. Yi, Y. Peng, ESRF-type lattice design and optimization for the High Energy Photon Source. Chin. Phys. C **2**, 027001 (2016). https://doi.org/10.1088/1674-1137/40/2/027001
15. S. Reiche, GENESIS 1.3: a full 3D time-dependent FEL simulation code. Nucl. Instrum. Methods Phys. Res. Sect. A **429**, 243–248 (1999). https://doi.org/10.1016/S0168-9002(99)00114-X
16. M. Borland, Simple method for particle tracking with coherent synchrotron radiation. Phys. Rev. Spec. Top. Accel. Beams **4**, 070701 (2001). https://doi.org/10.1103/PhysRevSTAB.4.070701
17. D. Xiang, G. Stupakov, Echo-enabled harmonic generation free electron laser. Phys. Rev. Spec. Top. Accel. Beams **12**, 030702 (2009). https://doi.org/10.1103/PhysRevSTAB.12.030702
18. Z. Huang, K.J. Kim, Formulas for coherent synchrotron radiation microbunching in a bunch compressor chicane. Phys. Rev. Spec. Top. Accel. Beams **5**, 074401 (2002). https://doi.org/10.1103/PhysRevSTAB.5.074401
19. L. Yu, Generation of intense UV radiation by subharmonically seeded single-pass free-electron lasers. Phys. Rev. A **44**, 5178 (1991). https://doi.org/10.1103/PhysRevA.44.5178
20. L. Yu, J. Wu, Theory of high gain harmonic generation: an analytical estimate. Nucl. Instrum. Methods A **483**, 493–498 (2002). https://doi.org/10.1016/S0168-9002(02)00368-6
21. D. Xiang, W. Wan, Generating ultrashort coherent soft X-ray radiation in storage rings using angular-modulated electron beams. Phys. Rev. Lett. **104**, 084803 (2010). https://doi.org/10.1103/PhysRevLett.104.084803
22. H. Li, Q. Jia, Z. Zhao, Generation of high harmonic free electron laser with phase-merging effect. Nucl. Instrum. Methods A **847**, 42–46 (2017). https://doi.org/10.1016/j.nima.2016.11.018
23. J. Rothhardt, S. Hädrich, J. Delagnes et al., High average power near-infrared few-cycle lasers. Laser Photonics Rev. **11**, 1700043 (2017). https://doi.org/10.1002/lpor.201700043
24. Y. Jiao, Z. Duan, Statistical analysis of the limitation of half integer resonances on the available momentum acceptance of the High Energy Photon Source. Nucl. Instrum. Methods A **841**, 97–103 (2017). https://doi.org/10.1016/j.nima.2016.10.037